Vol. 16, pp. 147–157 (2019)
doi: 10.2142/biophysico.16.0_147

Biophysics and Physicobiology

https://www.jstage.jst.go.jp/browse/biophysico/

Regular Article

Second harmonic generation polarization microscopy as a tool for protein structure analysis

Junichi Kaneshiro[1], Yasushi Okada[2,3], Tomohiro Shima[2,7], Mika Tsujii[4], Katsumi Imada[4], Taro Ichimura[1,5,6]* and Tomonobu M. Watanabe[1]*

[1]*Laboratory for Comprehensive Bioimaging, RIKEN Center for Biosystems Dynamics Research (BDR), Suita, Osaka 565-0874, Japan*
[2]*Laboratory for Cell Polarity Regulation, RIKEN Center for Biosystems Dynamics Research (BDR), Suita, Osaka 565-0874, Japan*
[3]*Department of Physics and Universal Biology Institute (UBI), Graduate School of Science, The University of Tokyo, Bunkyo-ku, Tokyo 113-0033, Japan*
[4]*Department of Macromolecular Science, Graduate School of Science, Osaka University, Toyonaka, Osaka 565-0043, Japan*
[5]*Transdimensional Life Imaging Division, Institute for Open and Transdisciplinary Research Initiatives (OTRI), Osaka University, Suita, Osaka 565-0871, Japan*
[6]*PRESTO, Japan Science and Technology Agency, Kawaguchi, Saitama 332-0012, Japan*
[7]*Present address: Department of Biological Sciences, Graduate School of Science, The University of Tokyo, Bunkyo-ku, Tokyo 113-0032, Japan*

Received April 1, 2019; accepted August 17, 2019

Cryo-electron microscopy and X-ray crystallography have been the major tools of protein structure analysis for decades and will certainly continue to be essential in the future. Moreover, nuclear magnetic resonance or Förster resonance energy transfer can measure structural dynamics. Here, we propose to add optical second-harmonic generation (SHG), which is a nonlinear optical scattering process sensitive to molecular structures in illuminated materials, to the tool-kit of structural analysis methodologies. SHG can be expected to probe the structural changes of proteins in the physiological condition, and thus link protein structure and biological function. We demonstrate that a conformational change as well as its dynamics in protein macromolecular assemblies can be detected by means of SHG polarization measurement. To prove the capability of SHG polarization measurement with regard to protein structure analysis, we developed an SHG polarization microscope to analyze microtubules in solution. The difference in conformation between microtubules with different binding molecules was successfully observed as polarization dependence of SHG intensity. We also succeeded in capturing the temporal variation of structure in a photo-switchable protein crystal in both activation and inactivation processes. These results illustrate the potential of this method for protein structure analysis in physiological solutions at room temperature without any labeling.

Key words: protein structure, structural variation, structure dynamics, SHG microscopy, label-free

* These authors made equal contributions and are both available for correspondence.
Corresponding authors: Taro Ichimura, Laboratory for Comprehensive Bioimaging, RIKEN Center for Biosystems Dynamics Research (BDR), 6-2-3 Furuedai, Suita, Osaka 565-0874, Japan. e-mail: ichimura@otri.osaka-u.ac.jp; Tomonobu M. Watanabe, Laboratory for Comprehensive Bioimaging, RIKEN Center for Biosystems Dynamics Research (BDR), 6-2-3 Furuedai, Suita, Osaka 565-0874, Japan. e-mail: tomowatanabe@riken.jp

◀ Significance ▶

Label-free optical modality using the second-harmonic generation (SHG) microscope reveals conformational variation of proteins and their dynamics under physiological conditions. A conformational change of microtubules (MTs) is detected through the SHG tensor analysis. A phenomenological model for an MT suggests that the electric dipole moment in each tubulin slightly tilts outward on taxol binding. A time development of an SHG tensor of a crystal of photo-switchable fluorescent protein Kohinoor is successfully observed both in activation and inactivation processes. Compared with two-photon fluorescence measurement, the polarization dependence of SHG intensity shows unique features indicating structural change of Kohinoor on photo switching.

For many decades, the major tools of protein structure analysis have been cryo-electron microscopy (cryo-EM) and X-ray crystallography [1,2], both of which are currently advancing to the next generation [3,4]. Although cryo-EM and X-ray crystallography provide static information on protein structure, structural dynamics can be investigated using nuclear magnetic resonance (NMR) and Förster resonance energy transfer (FRET) [5,6]. These technologies provide a comprehensive tool-kit for the analysis of protein structures. However, these tools present several important practical difficulties such as preservation of biological samples in a frozen-hydrated state prior to examination using an electron microscopy grid in cryo-EM observations, requirement of a highly-purified single crystal with a typical size of 30–300 μm for X-ray crystallography; and chemical labeling for NMR and FRET. Here, we propose bypassing the problems mentioned above by adding the measurement of second-harmonic generation (SHG) polarization to the tool-kit of structural analysis methodologies.

In biology, SHG microscopy is a powerful modality that enables the visualization of fiber structures, such as the fibrillar collagen in tendons, myosin thick filaments in muscle sarcomeres, and the densely bundled microtubules in living specimens [7–9]. The nonlinear susceptibility of a material to SHG is expressed as the 3rd-rank tensor (SHG tensor) originating from molecules with broken centrosymmetry and their alignments in macromolecular assemblies [7,8]. This unique feature provides information about protein secondary structures, such as the axial pitch of collagen helices [10], and visualizes the spatial distribution of fiber polarity directions in tissues with interferometric configurations [11,12]. Therefore, the SHG signal potentially carries structural information about proteins, which can be recorded optically without labeling. In contrast to the pre-existing tools, SHG signals can be easily measured in the physiological condition without the need of freezing or ultrahigh vacuum. Also, SHG requires only a small crystal or fabric structure with a sub-micrometer volume determined by the diffraction limit of excitation light (ca. 200–500 nm for near-infrared lasers). Once the relationship between SHG response and the protein structure provided by cryo-EM or X-ray crystallography is revealed, one can understand spatio-temporal changes of the structure under the physiological condition from the SHG analysis in combination with the *a-priori* knowledge of the structure. Therefore, SHG microscopy enables us to link the biological functions to protein structures.

In order to prove this concept, we investigated the feasibility; (1) that the structural variation of a protein is measurable with SHG microscopy; and (2) that SHG microscopy enables the tracking of dynamic structural changes in a small protein crystal. Microtubule (MT), a tubular cytoskeletal polymer protein composed of heterodimers of α- and β-tubulin [13–15], was employed for the first investigation, because the structural variation of MT has been studied extensively [16–19]. In this paper, we demonstrated the estimation of electric dipole moments in tubulin subunits (α- and β-tubulins) reflecting structure difference in MT from the incident polarization dependence of SHG intensity. Although this method has already been applied to investigate a biophysical phenomenon [20], the relationship between protein structure and SHG measurement was not discussed in detail. For the second investigation, we employed a photo-switchable fluorescent protein, Kohinoor, whose chromophore structure can be easily switched by the irradiation of lights at specific wavelengths [21]. The dynamic change of the chromophore structure could be observed as the time development of SHG polarization dependence of a protein crystal, providing a tool that complements crystallography. This study exhibits the potential of SHG polarization measurement as a tool to complement the drawbacks of current structural analysis methods.

Materials and Methods

Construction of the SHG microscope

Polarization-resolved SHG measurements were performed using a purpose-built laser-scanning SHG microscope in the transmission geometry with a polarization-control device in the incident light pathway (Fig. 1A). The microscope has a mode-locked Ti:sapphire laser (Chameleon Vision II, Coherent, Santa Clara, California, USA) with a wavelength of 810 nm, a repetition rate of 80 MHz, and a pulse duration of 200 fs as an excitation light source. The laser beam was introduced to a Glan Laser polarizing prism (GL10-B, Thorlabs, Newton, New Jersey, USA) and a high-speed polarization controller composed of a pair of electro-optic modulators (EOMs) (Model 350-160, Model 350-80, Conoptics, Danbury, Connecticut, USA) [22], which will be explained in more detail in the next section. The beam was deflected by an *X*–*Y* scanner consisting of a pair of galvano mirrors (VM500+, GSI, Bedford, Massachusetts, USA), and was focused using a dry objective lens with a numerical aperture (NA) of 0.95 and a magnification of 40 (CFI Plan Apo Lambda, Nikon, Tokyo, Japan). The SHG signal emitted in the forward direction was collected using another oil-immersion objective lens with an NA of 1.45 and a magnification of 100 (CFI Apo, Nikon), and detected using a photon-counting photomultiplier tube (PMT) module (H10680-210, Hamamatsu Photonics, Shizuoka, Japan) after passing through a short-pass filter (FF01-680/SP, Semrock, Rochester, New York, USA) and a band-pass filter (FF01-405/10-25, Semrock). A branch of the SHG detection path is also constructed as a "calibration path", which is separated by a removable silver mirror located between a lens and a band-pass filter. The usage of this path is described in the next section.

Calibration of incident polarization state

We used a linearly polarized laser to measure the incident-

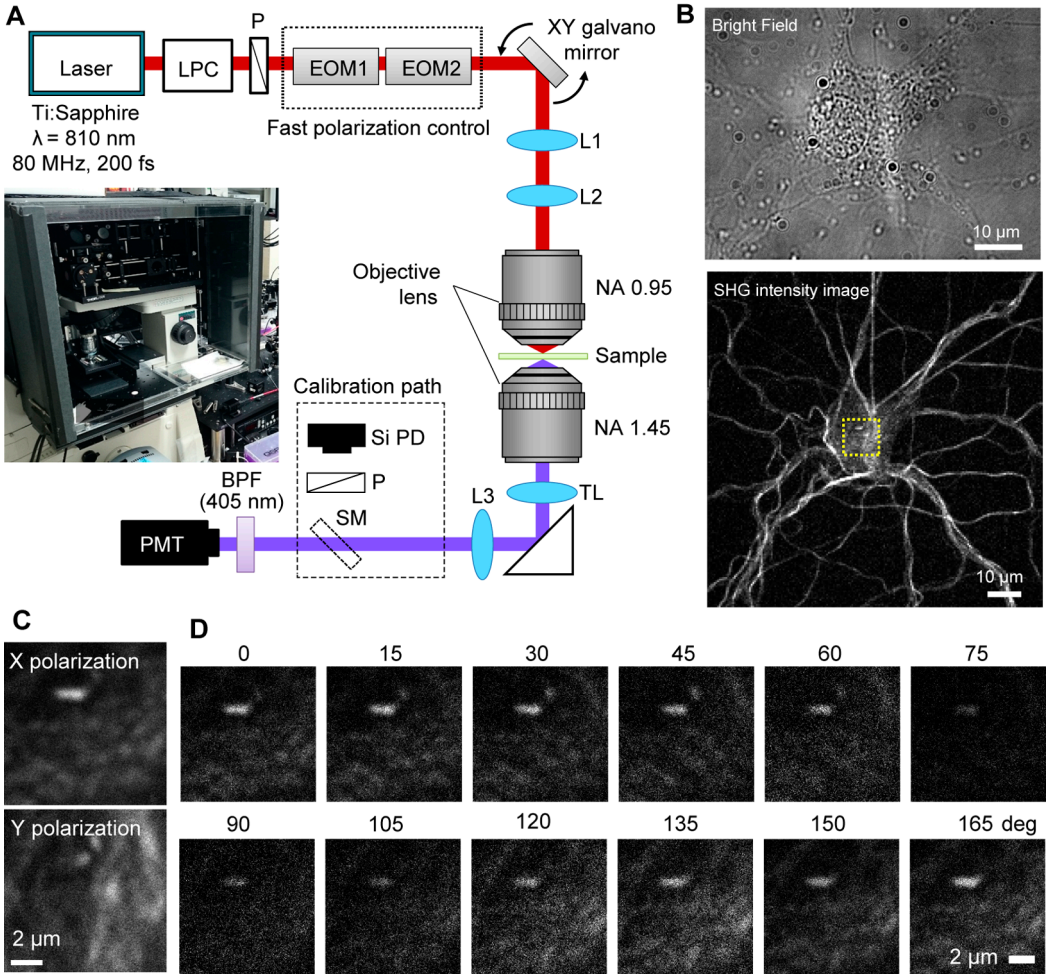

Figure 1 SHG polarization measurement. (A) Schematic drawing of the present SHG microscope. LPC, Laser power controller; P, polarizer; EOM1 and EOM2, electro-optic modulators; L1, L2, and L3, achromatic lenses; TL, tube lens; M, mirror; SM, removable silver mirror; SiPD, Si photodetector; PMT, photomultiplier tube; BPF, bandpass filter; NA, numerical aperture. The inserted photo is the present microscope combined with an incubator to stabilize MT polymerization. (B) Brightfield image (*upper*) and SHG image (*lower*) of a fixed nerve cell. MTs in the cell were fixed with paclitaxel (taxol) followed by extraction of other proteins and organelles using Triton X-100. (C) Enlarged image of *X*- (*upper*) and Y-polarization (*lower*) in the region indicated by the yellow rectangle in (B). (D) Incident polarization dependence in *X*-polarization in SHG.

polarization dependence of SHG intensity. In principle, any state of polarizations can be produced by applying appropriate control-voltages to the drivers of EOMs [22]. The two EOMs, EOM1 and EOM2, were used to control the orientation and ellipticity of the polarization states, respectively. To measure the incident-polarization dependence, we needed to sweep the orientation of linear polarization with the ellipticity fixed to zero. To achieve this condition, we determined a constant control-voltage to the EOM2 driver (V_{20}), which minimizes the ellipticity to ideally zero, and also determined two other parameters V_{10} (offset voltage of EOM1) and V_π (half-wavelength voltage of EOM1) at the sample stage position as a function of the control voltages (V_1, V_2) with a small step-size. From this data, we were able to find the V_{20} value for the minimum ellipticity and recorded the polarization state at $V_2=V_{20}$. However, because of the instability of the experimental environment (e.g. temperature and humidity), we could not use the same value for V_{20} (also V_{10} and V_π). Therefore, the polarization state had to be checked before every experiment to ensure the polarization state is linear (ellipticity=zero) at the sample stage. We used the calibration path (Fig. 1A) for routine checkup instead of precisely measuring the polarization state, which required the rearrangement of optical configuration. When V_1 is swept with V_2 fixed, the output intensity of the calibration path varies with a sinusoidal form as $I_0[1+A\cos(\pi(V_1-V_{10})/V_\pi)]$, where I_0 is a constant, A is a variable dependent on the ellipticity, i.e. V_2. The parameters (I_0, A, V_{10} and V_π) are determined at a certain V_2. We determined a reference value of A (denoted by A_0) as a corresponding value to V_{20} in advance. In the routine checkup, a V_2 value, which gave A_0, was selected as optimum V_2 providing the minimum ellipticity. The V_{10} and V_π values were also determined by the least squares fitting at every experiment.

Tubulin preparation

Tubulin was purified from a porcine brain through four cycles of polymerization and depolymerization using 1 M PIPES buffer (1 M PIPES-KOH, 1 mM EGTA, 1 mM $MgCl_2$, pH 6.8) for the effective removal of microtubule-associated proteins [23]. Some tubulin was labeled with red florescent dye, Alexa Fluor 647 (A-20106, Thermo Fisher Scientific, Waltham, Massachusetts, USA) following the previously reported protocol [24]. We used a mixture of the labeled tubulin and the non-labeled tubulin to check the adsorption and alignment of microtubules before SHG measurements.

Preparation of microtubule bundles for observation

Xenopus egg extract and demembranated sperm heads were prepared as reported previously for the investigation of MT bundles [25]. The reactions were conducted at 37°C in rectangular flow channels with a typical width of 1.2 mm, a height of 30 μm, and a length of 18 mm, then formed between two coverslips according to the following procedure (Supplementary Fig. S1). The demembranated *Xenopus* sperm was incubated for 5 min in the flow channel. The floating sperm was washed with 5 μL of 7 mg/mL casein dissolved in 50 mM PIPES-KOH, 2 mM $MgSO_4$, and 1 mM EGTA; pH 6.7 (PEM). *Xenopus* egg extract (5 μL) was added and the mixture was incubated for 10 min to create microtubule organizing centers. Excess egg extract was removed by washing with 5 μL of warmed high-concentration PIPES buffer (500 mM PIPES-KOH, 10 mM $MgCl_2$, 5 mM EGTA, pH 6.94) and 10 μL of warmed PEM with 30% (v/v) glycerol (PEM-glycerol). Tubulin (8 μL, 15 μM) purified from porcine brain was loaded and incubated for 20 min in PEM with 1 mM GTP and 1 mg/mL casein. The polymerized microtubules were bundled by the flow of 20 μL of PEM-glycerol. For the taxol-bound MTs, the washing buffer replaced 20 μL of PEM-glycerol with 10 μM taxol.

Polarization-resolved SHG imaging of microtubule bundles

A set of polarization-resolved SHG images was obtained by synchronous control of the *X*-*Y* scanner and the polarization controller. The laser focus was raster-scanned in a 50×50 μm^2 square with a pixel pitch of 500 nm (100×100 pixels) and a dwell time of 13 ms. The incident polarization was swept within the dwell time at every pixel position. The angle pitch was 7.5° and the number of angles was 26, which covered a total angle range of over 180°. The total time required to obtain a whole image set was 130 s. The average laser power at the focal plane was approximately 30 mW.

Estimation of dipole angle of a tubulin subunit from the incident polarization dependence of SHG

The SHG intensity in an area that covered an entire bundle at each polarization-resolved image was integrated to obtain one set of polarization-dependent data for one bundle. The number of integrated pixels for a set of data was in the range 100–2000 depending on the size of the bundle. The polarization-dependent data were then fitted using the following theoretical function of incident polarization angle θ with three fitting parameters α, χ_{zzz} and χ_{zxx}.

$$I(\theta;\alpha,\chi_{zzz},\chi_{zxx}) = \{\chi_{zzz}\cos^2(\theta-\alpha)+\chi_{zxx}\sin^2(\theta-\alpha)\}^2 + \{2\chi_{zxx}\cos(\theta-\alpha)\sin(\theta-\alpha)\}^2 \quad (1)$$

I indicates integrated signal read by the PMT and α denotes the average orientation angle of an MT bundle. Angles θ and α were defined according to the Y laboratory axis (Fig. 2A). Parameters χ_{zzz} and χ_{zxx} are two components of the SHG susceptibility tensor. Precisely, Eq. 1 should be multiplied by an instrument constant I_0, which depends on system factors such as the intensity of incident laser, attenuation coefficient of the entire optical system from detecting objective lens to the PMT. However, here we omitted I_0 and treated χ_{zzz} and χ_{zxx} as values including I_0 since only the ratio between χ_{zzz} and χ_{zxx} is important in the present paper. Equation 1 is equivalent to a well-established form of SHG polarization dependence in biological filaments [26].

We herein describe how to estimate the effective tilt angle (φ) of tubulin subunits from the parameters χ_{zzz} and χ_{zxx} (Fig. 2C). The z-axis is defined as the direction parallel to the central axis of the MT, and the x- and y-axes are defined as perpendicular to the MT axis. Assuming cylindrically symmetric alignment of the tubulin, χ_{zzz} and χ_{zxx} are the only two independent non-zero components that express all other non-zero components. We applied Kleinman's law [7] because the wavelengths used in our measurements were far from the absorption wavelength of proteins in an MT. The two components are related to φ by the following equations:

$$\chi_{zxx} = K\left(\frac{\beta}{2}\right)\cos\varphi\sin^2\varphi$$

$$\chi_{zzz} = K\beta\cos^3\varphi \quad (2)$$

K is a constant that is proportional to the net molecular number in the focal volume. Although each tubulin subunit has a hyper-polarizability tensor, we employed the dominant hyper-polarizability, β, which is defined as a component of the hyper-polarizability tensor along the permanent dipole moment of a tubulin subunit that produces the highest nonlinear polarization. The effective tilt angle (φ) has the following relationship with the ratio of χ_{zzz} and χ_{zxx}:

$$\frac{\chi_{zxx}}{\chi_{zzz}} = \frac{1}{2}\tan^2\varphi \quad (3)$$

Thus, we estimated the effective tilt angle φ, throughout this study, based on the values of χ_{zzz} and χ_{zxx} extracted from the curve fitting Eq. 1 to the experimental results.

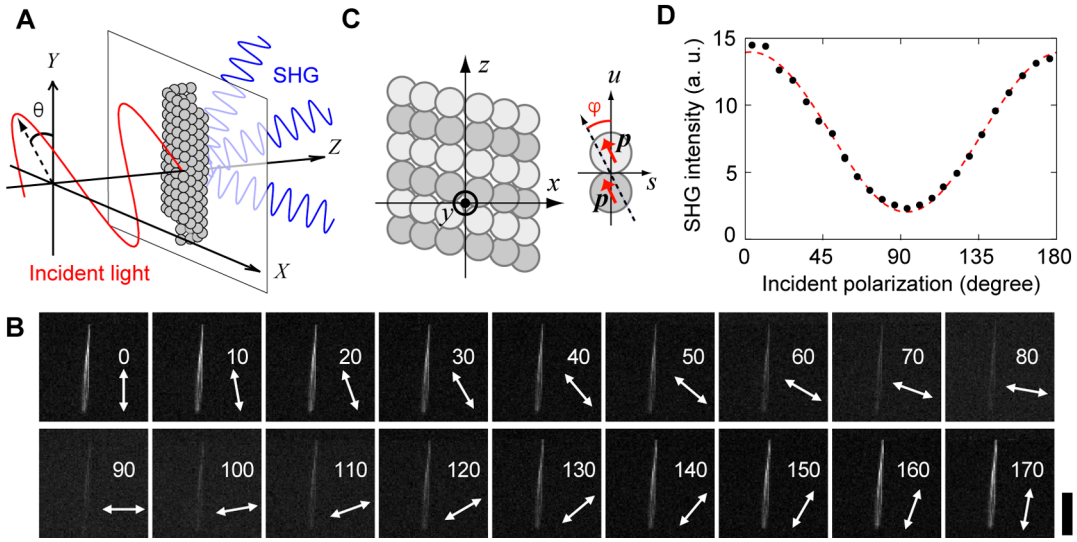

Figure 2 SHG polarization measurement of an MT bundle. (A) Orientation of an MT and incident polarization θ defined in the *XYZ* laboratory coordinate system. (B) SHG images of an MT bundle at incident polarizations in the range 0°–180° as indicated by the arrows. (C) Definition of axes and angle φ in an MT. The intra-tube axes *z* and *x* (*y*) are parallel and perpendicular to the MT axis, the intra-tubulin axes *s* and *u* are radial from and parallel to *z*, and φ is the tilt angle of tubulin subunits, ***p***, from the *z* axis (See also Supplementary Fig. S4). (D) A typical polarization dependence of SHG intensity of an MT bundle. Red dashed line, theoretical curve obtained by the least-squares fitting of Eq. 1. The scale bar is 10 μm.

Crystallization of photo-switchable fluorescent protein Kohinoor

The cDNAs for positively photo-switchable protein, Kohinoor, kindly provided by Prof. T. Nagai, were inserted into an *Escherichia coli* expression vector pAL7 (BIO-RAD, Hercules, California, USA) and transformed into the *E. coli* strain Rosseta2 (DE3) (Merck Millipore, Burlington, Massachusetts, USA). The expressed Kohinoor was purified using a Profinity eXactTM Fusion-Tag system (BIO-RAD) following the protocol recommended by BIO-RAD. The yield of purified Kohinoor was 3–4 mg. Then the Kohinoor solution was concentrated to 8 mg/mL in 1 mM 4-(2-hydroxyethyl)-1-piperazineethanesulfonic acid (HEPES) (pH 7.5) using Amicon Ultra Centrifugal Filters (Merck Millipore).

The purified Kohinoor was crystallized using the hanging-drop vapor-diffusion technique. The Kohinoor proteins were precipitated and crystalized within 1 day at 20°C from drops prepared by mixing 1.2 μL of the protein solution with 1.2 μL of a reservoir solution comprising 50 mM HEPES (pH 8.0), 10% PEG4000, and 26.7 mM $MgCl_2$.

SHG observation of Kohinoor crystal

We introduced a 395/470-nm LED light source (Light Engine Spectra, Lumencor, Beaverton, Oregon, USA) to activate and inactivate Kohinoor, and a band-pass filter (FF01-525/45-25, Semrock) for fluorescence observation, into the present SHG microscope. Small pieces of Kohinoor crystal were loaded into a glass chamber with the buffer (phosphate-buffered saline). The SHG signal of the Kohinoor crystal was recorded using the same procedure used for the polarization dependence measurement of the microtubule bundles, except that the dwell time was 1.0 ms and the number of polarization angles was 25.

For comparison of the polarization dependence of total SHG intensity between fluorescent and non-fluorescent states, the sequence of [10 s irradiation of 470 nm light at 0.43 mW, SHG recording, 10 s irradiation of 395 nm light at 0.16 mW, SHG recording] was repeated 10 times. For time course measurements of the incident polarization dependences during 470 nm light irradiation for activation (or during 395 nm light irradiation for inactivation), the sequence of [1.0 s irradiation of 470 nm light at 0.43 mW, SHG recording] (or [1.0 s irradiation of 395 nm light at 0.016 mW, SHG recording]) was repeated 10 times.

Phenomenological model fitting the SHG observations of the Kohinoor crystal

We assumed that the space group of our Kohinoor crystal samples was $P2_12_12$ according to a report of the crystal structure of a similar positively photo-switchable protein, Padron, into which some mutations were introduced to develop Kohinoor [21]. The SHG tensor under this symmetry condition has only three components (χ_{xyz}, χ_{yzx}, and χ_{zxy}) in the tensor principal coordinate system (*x*,*y*,*z*) [27]. We introduced an imaginary part into each component of the SHG tensor to adjust for the effect of resonance on SHG, because the SHG wavelength in the present measurement system (405 nm) was within the absorption band of Kohinoor.

The polarization dependence of the total SHG intensity was expressed as

$$I(\theta, \eta, \zeta, p_1, p_1) = \frac{1}{2}[\cos^2(\theta-\eta)\{p_1+p_2-(p_1-p_2)\cos^2(\theta-\eta)\}\sin^2(2\zeta)], \quad (4)$$

where η and ζ denote the orientations of the sample (Supplementary Fig. S2), and p_1 and p_2 are material-dependent parameters expressed with χ_{xyz}, χ_{yzx}, and χ_{zxy} by the following equations.

$$p_1 = (\chi'_{xyz}+\chi'_{zxy})^2 + (\chi''_{xyz}+\chi''_{zxy})^2,$$
$$p_2 = (\chi'_{yzx})^2 + (\chi''_{yzx})^2 \quad (5)$$

The single and doubled primes represent real and imaginary parts, respectively. The derivations of Eqs. 4 and 5 are provided in the Methods section in the Supplementary Text S1. According to Eqs. 4 and 5, the complexity of the resonance effect was invisible under the experimental conditions when we measured total intensity. Moreover, only two real positive values of p_1 and p_2 were significant and beneficial to a discussion of the patterns of the polarization dependence curves of SHG from the Kohinoor crystal. Because the values of p_1 and p_2 can be uniquely determined as long as $\sin^2(2\zeta)$ is not zero, we assumed $\zeta=\pi/4$ in the present study.

In the SHG signal obtained, $I(\theta)$ comprises the polarization dependence of pure SHG intensity, $I_{SHG}(\theta)$, and that of fluorescence, $I_{fl}(\theta)$, as

$$I(\theta) = I_{SHG}(\theta) + c \times I_{fl}(\theta), \quad (6)$$

where c is a dimensionless parameter. The effect of fluorescence can be removed by using this equation with $I_{fl}(\theta)$ detected at 525 nm. Hence, the parameters, η, p_1, p_2, and c, were estimated by fitting $I_{SHG}(\theta)$ with Eqs. 4 and 6 (Supplementary Fig. S3).

Results

Estimation of dipole angle of a tubulin subunit from the incident polarization dependence of SHG

We designed and developed a SHG microscope with a rapid polarization control device comprising a pair of EOMs (Fig. 1A) as previously reported [22]. The SHG microscope enables measurement of the intensities of SHG light at various incident polarization angles. While observing a fixed nerve cell, the bundled MTs were selectively observed in the dendrites (Fig. 1B), and the centrosome, whose electric polarization arises from oriented microtubules, was also visualized using the present SHG microscope (Fig. 1C and D).

To investigate the feasibility of measuring the structural variation of proteins with SHG microscopy, we used dense bundles of parallel microtubules (MT bundles) whose SHG intensity is proportional to the square of the number of tubulin subunits in a focal volume. Hundreds of microtubules were grown in a *Xenopus* egg extract from the sperm head, which served as the artificial microtubule-organizing center [28] (Supplementary Fig. S1, and see the Materials and Methods section). The SHG intensity emitted from an MT bundle adsorbed on glass surface clearly depending on the incident polarization (Fig. 2B and D). The angle of a permanent dipole moment in a tubulin subunit (φ) was defined as the tilting angle from the central axis of the MT cylindrical structure (Fig. 2C) and the dominant hyper-polarizability, which is derived from only two independent components of the SHG tensor (χ_{zzz} and χ_{zxx}) (Supplementary Fig. S4, and see the Methods section), as previously described [26]. Practically, the value of φ was calculated by fitting the incident polarization dependence of SHG intensity with the theoretical function (Fig. 2D).

We measured the φ values of each pixel on an MT bundle extended by adding guanosine diphosphate (GDP), termed GDP-MT, and generated a histogram of the φ values (Fig. 3A). The mean φ was estimated to be 38.5° by fitting the histogram with a Gaussian function (Fig. 3A). Taxol (paclitaxel) is known to induce the structural change of MTs to inhibit depolymerization [18]. The mean φ of the taxol-stabilized GDP-MT, termed GDP-taxol-MT, was estimated to be 39.7° (Fig. 3B), suggesting that taxol modifies the tilt angle of GDP-bound MT with respect to the tube axis. The distributions in Figure 3A and Figure 3B came from measurement noise dominated by photon counting statistics in the present optical setup. Standard errors for GDP-MT (Fig. 3A) and for GDP-taxol-MT (Fig. 3B) were 0.030° and 0.037° respectively, which are significantly smaller than the difference of the mean values (1.2°). The statistical significance was also evaluated by the Student's *t*-test, and indicated in Figure 3C.

For the MTs composed of crudely purified tubulins decorated with MT-binding proteins (MTBPs), such as microtubule-associated proteins, the estimated dipole moment angles were slightly larger and smaller for GDP-MT (38.7°) and GDP-taxol-MT (39.3°), respectively (Fig. 3C), compared with those of the finely purified tubulins. This small shift indicated that the average dipole angle of the MTBP is between the average dipole angles of the two states of tubulin. Accordingly, we shifted the estimates of the effective angle toward the dipole of the MTBP (Fig. 3D). Thus, we successfully detected the structural variation in an MT bundle with the SHG polarization measurement.

Temporal structural analysis in a crystal of photo-switchable fluorescent proteins

We next examined the feasibility of a time-lapse observation of structural changes in a protein crystal. Photo-induced conformational change is one of the best models of the dynamic phenomenon because the timing of the conformational changes can be easily and precisely controlled by light irradiation. We here chose Kohinoor as a model sample. It is a positive photo-switchable fluorescent protein with a high

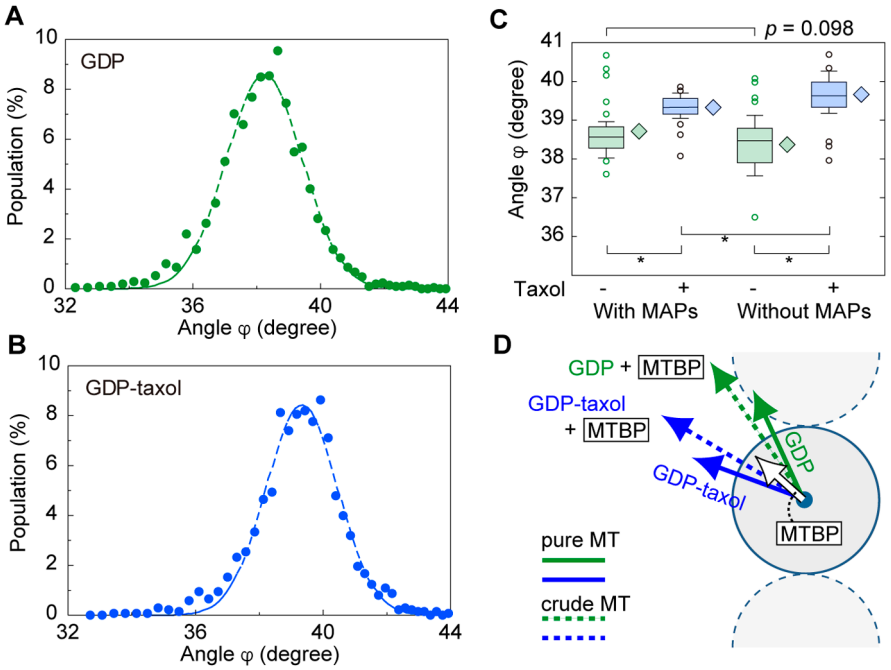

Figure 3 Structure analyses of MT bundles by polarization SHG microscopy. (A, B) Histograms of estimated φ for GDP-MT (A, N=2095 in 24 bundles) and GDP-taxol-MT (B, N=1378 in 29 bundles) composed of pure tubulins. The broken lines are fitting results with a Gaussian function. (C) Boxplots of the average φ in GDP-MT (*green*) and GDP-taxol-MT (*blue*) bundles composed of pure (*left*) and crudely purified tubulins (*right*). N=24, 29, 43, and 46 bundles. Asterisks indicate $p<0.01$ (Student's t-test). (D) Interpretation of measured dipole angles shown in (C). Solid and dotted arrows (*green*: GDP-MT, *blue*: GDP-taxol-MT) indicate the dipoles of MTs composed of pure tubulins and crudely purified tubulins, respectively. The white arrow indicates the estimated dipole for MTBP.

switching rate and high photo-stability [21]. The chromophore of Kohinoor is activated to a fluorescent state (active state) by 470-nm irradiation, and inactivated to a non-fluorescent state (inactive state) by 395-nm irradiation (Fig. 4A).

The Kohinoor did not lose the photo-switchable ability even when crystalized (Fig. 4B). Both the intensity of the SHG signal and its polarization dependence differed markedly between the active and inactive states when recorded in repeated cycles of activation and inactivation (Fig. 4C and D). The observed SHG signal also contained two-photon excited fluorescence. The polarization dependence of the fluorescence was significantly different from that of SHG, and there was no difference between the two states (Fig. 4E). This result indicates that the difference in the observed polarization dependence originated not from fluorescence but from SHG, owing to the structural differences in a Kohinoor crystal. We predict that the difference between fluorescence and SHG comes from the difference of physical origins of the phenomena, however, this is still a remaining issue to be solved in further studies.

Importantly, the present method enabled tracking of the dynamic change in both the activation and inactivation processes. While observing the activation process, the polarization dependence curve gradually changed, most likely in a single-phase manner (Fig. 5A). Meanwhile, in the inactivation process, the change of the polarization dependence curve exhibited a two-phase manner: two peaks became one peak in only 2 frames (2 s) and gradually decreased (Fig. 5B). According to this result, the state transition of Kohinoor molecules in a crystal is thought to follow different pathways on the activation and on the inactivation. As such, the dynamic information cannot be directly obtained by static structural analysis like X-ray crystallography.

Finally, we tried to more quantitatively evaluate the state transitions observed here. We constructed a phenomenological model based on the crystal lattice structure of the progenitor of Kohinoor, Padron [29], because the crystal structure of Kohinoor has not been reported yet. According to the model, two positive real parameters—p_1 and p_2—are defined as beneficial variables to describe the pattern of polarization dependence of SHG in the Kohinoor crystal (see the Materials and Methods section and the Methods section in the Supplementary Text S1 for details). The state transition of a Kohinoor crystal has been successfully represented using these parameters estimated through SHG tensor analysis (Fig. 5C and Supplementary Fig. S3).

Discussion

We have demonstrated the potential of SHG microscopy as a structural analysis tool. Some literature on the application

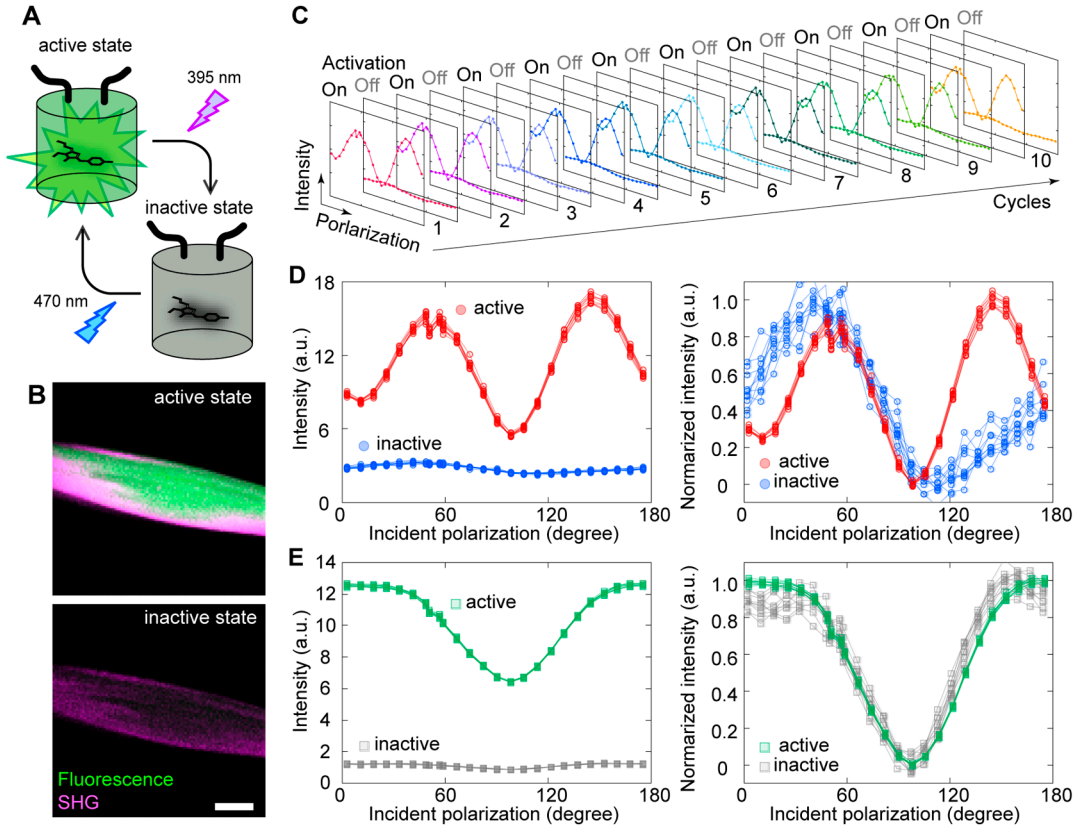

Figure 4 Time-lapse measurements of SHG and fluorescence in a Kohinoor crystal. (A) Schematic of a state transition in photo-switchable protein, Kohinoor. (B) SHG (*magenta*) and fluorescence (*green*) images of a Kohinoor crystal in the active state (*left*) and the inactive state (*right*). The scale bar is 20 μm. (C) Repeated measurement of polarization dependence of SHG in a Kohinoor crystal between the active and inactive states. We obtained the fluorescence signal with the SHG measurement. (D) Typical 10 traces of the polarization dependence of SHG in the active state (*red*) and the inactive state (*blue*). Left, raw data; Right, normalized data from 0.0 to 1.0 to the minimum and maximum of the average of the 10 trials. (E) Typical 10 traces of the polarization dependence of fluorescence in the active state (*green*) and the inactive state (*grey*). Left, raw data; Right; normalized data from 0.0 to 1.0 to the minimum and maximum of the average of the 10 trials.

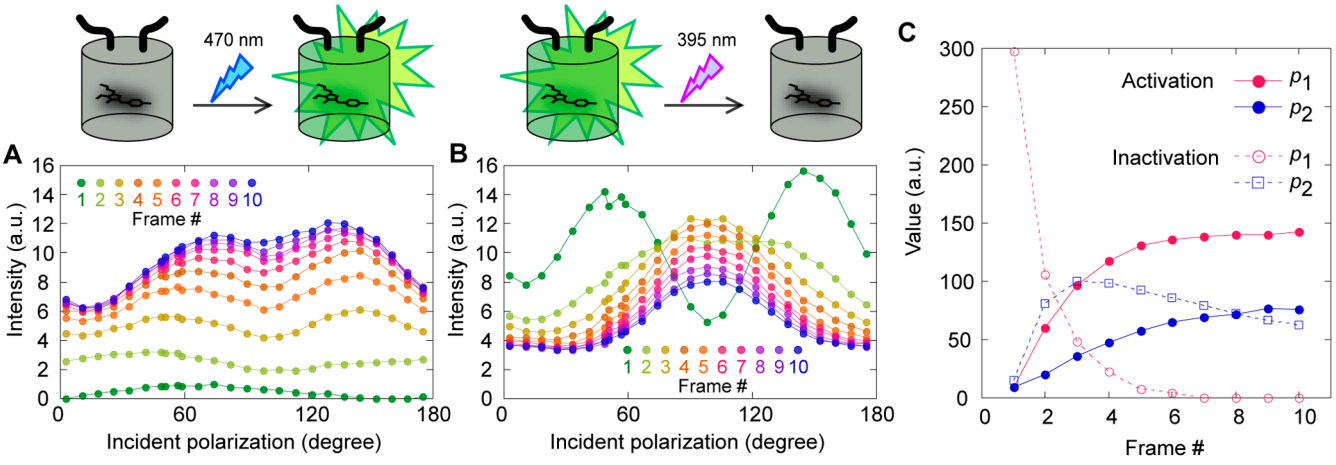

Figure 5 Temporal structural analysis in a protein crystal of photo-switchable fluorescent proteins. (A, B) Time developments of the incident polarization dependence curves during 470-nm irradiation (A) and 395-nm irradiation (B). Colors from green to blue indicate the frame number from 0 to 10. (C) Time courses of results fitted to the phenomenological model (Eq. 4, see Materials and Methods section for details). *Red closed circles*, p_1 in activating process; *Blue closed circles*, p_2 in activating process; *Red open circles*, p_1 in inactivating process; *Blue open squares*, p_2 in inactivating process.

of the polarization-resolved SHG has been previously published, especially on MTs, for example, the degree of alignment of MTs in a bundle [30,31], tau-binding to MT [30,32], and so on. In contrast to these works, this study successfully demonstrates that SHG can detect the structural change on the inside of a protein of interest.

In the present study, the taxol addition to MTs caused the significant difference in dipole angle φ (Fig. 3A and B). This result is inconsistent with the previous report that the taxol addition does not affect SHG polarization of MTs in a retinal flat mount [33]. Because the MTs used were dissociated from retinal flat mount by the addition of nocodazole, which is a chemical agent that inhibits tubulin polymerization, the MTs seem to be highly decorated with many kinds of associated proteins. Meanwhile, the MTBPs decreased the difference between MT structures with and without taxol in the present study (Fig. 3C). Therefore, the structural change due to the taxol addition could be small enough to hide the electrical polarity of the associated proteins in crude isolated MT bundles. In a previous study, the associated protein, mainly tau proteins, were not removed [26]. A remarkable achievement of the present study is that we successfully evaluated the structural difference in pure MTs themselves using SHG microscopy.

The validity of the present estimation of the dipole angle φ (Fig. 3) deserves further discussion. In the present study, the local coordinate system (s,t,u) was independently defined in each protofilament from the principal system (x,y,z) (Supplementary Fig. S4A). The local axes s and t were set to radial and azimuthal directions at the location of the corresponding protofilaments, and the u axis was parallel to the MT axis (u//z). In general, the three-dimensional orientation of a dipole $\boldsymbol{p}$ in a tubulin subunit can be expressed by two angle parameters: φ and δ (Supplementary Fig. S4B). The former parameter (φ) is, as previously mentioned, defined as the angle between u and $\boldsymbol{p}$, whereas the latter (δ) is the orientation of $\boldsymbol{p}$ within the st plane (= xy plane). Because an MT has rotational symmetry about the z-axis, all protofilaments have the same axial dipole component (p_A). Therefore, it is only necessary to discuss the lateral component p_L with regard to the SHG tensor for the entire microtubule. Nine examples of possible alignments of p_L projected in the xy plane are illustrated (Supplementary Fig. S4C). The SHG tensor for an MT is calculated as the summation of the local SHG tensors for the protofilaments. Since the diameter of MT is much smaller than the wavelength used in this study, the difference regarding δ vanishes as a result of integration, even if the configuration of the dipole array varies as a function of δ. In a microscopic view, a contribution of a tubulin subunit to the SHG tensor component χ_{zxx} is proportional to $p_A p_L^2$ [34], thus the effect of p_L is not canceled out but remains after integration over all tubulin subunits in an MT. In principle, it is possible to obtain only a φ value. In the present experimental assay, some MTs in a bundle are possibly adsorbed on the surface of the glass while others are not. Effects of adsorption on MT structure, especially on its rotation symmetry, are still unknown. However, we used an MT bundle in which most MTs are not in contact with the glass surface, thus, the rotational symmetry is conserved for an average MT structure. The MTs in a bundle are not necessarily oriented in the same direction. Dispersion of MT orientations in a bundle may affect the estimation result of φ. However, we have confirmed by calculation that the effect can be almost ignored (Supplementary Fig. S5).

The present method can only obtain the summation of dipoles of each component within an optical confocal volume. Assuming that: (i) MTBPs on average exhibit a permanent dipole; (ii) the permanent dipoles of tubulin subunits and MTBPs are independent of each other, the total SHG tensor (χ_{total}) is expressed as the sum of the SHG tensors of MT (χ_{MT}) and of MTBPs (χ_{MTBPs}); and (iii) MTBPs are uniformly distributed over the entire surface of the MT with rotational symmetry (Supplementary Fig. S4C). As discussed above, the contribution of χ_{MTBPs} is thought to originate from an average dipole of MTBP with some specific angle φ. Because the lateral orientations of the dipoles make no contribution to the resultant SHG tensor components, it is possible to visualize a simplified situation in which all the dipoles exist in the same plane (the su plane in Supplementary Fig. S4B and Fig. 3D). According to the experimental results (Fig. 3C), the orientation of the MTBP dipole (Fig. 3D, *white*) must exist in the range between those of GDP-MT (Fig. 3D, *green*) and GDP-taxol MT (Fig. 3D, *blue*). Because the structural difference between GDP-MT and GDP-taxol-MT is minimal, the dipoles of the two structures can be considered equivalent in magnitude. Hence, we determined the angle of the MTBP dipole to be 38.9° and the magnitude to be 1.00-fold that of the MTs (see Supplementary Text for detail of estimation). Hence, the present methods can be capable of detecting the attachment/detachment of proteins on a protein filament.

The MT is a cytoskeletal rail protein-complex on which kinesin and dynein motor proteins walk, and the motor proteins binding also possibly induces the structural change of β tubulin in GDP-MTs [18,19]. We previously reported that the addition of kinesin into solution results in a higher value of the estimated φ [20]. The φ value was not proportional to the kinesin concentration, but it exhibited sigmoid response as a function of kinesin concentration [20]. This previous result clearly indicated that the polarity of kinesin was not dominant in the SHG polarization measurement, but the SHG microscopy detected the re-orientation of the dipole moment in αβ tubulin dimers, most likely allosterically, inducted by kinesin binding. In addition to the previous study, the present study is proof that the internal structural change in a protein is certainly detectable with SHG microscopy.

We represented the structural dynamics in a Kohinoor crystal with two parameters based on the phenomenological model (Fig. 5C). Considering the common mechanism

displayed by Dronpa-based photo-switchable fluorescent proteins [35,36]—in which the benzene ring in the chromophore is dynamically flipped through a *cis–trans* transition—the same phenomenon might contribute to the change in the polarization dependence of SHG. More information about the crystal structure of Kohinoor leads to a better understanding of the relationship between these parameters and the structural change of the chromophore in Kohinoor. It should be noted that the sample we used her was a protein crystal, applicable to X-ray crystallography. In the present study, unfortunately, the purity of the single crystal of Kohinoor used was not sufficient for X-ray crystallography. Thus, detailed interpretation remains for future studies.

Meanwhile, the Kohinoor experiments also demonstrated the high usability of SHG for structure analysis. Preparation of high-purity protein crystals is often time-consuming. Before investigating structural difference with X-ray crystallography, it is possible to examine whether the structure of interest is certainly differed or not by using the present method. The present method is very convenient as a tool for easy preliminary investigation before the precise structural analyses.

Conclusion

SHG was first discovered in 1961 as a nonlinear optical process, in which two photons of the same energy are combined into a new photon of twice the energy [37]. Since the first discovery, SHG has been utilized to visualize fiber structures in cells as a label-free modality [7–9], to measure the action potential of a nerve cell as an electrical susceptible modality [38,39], and to observe the deep area in a tissue or animal as a near-infrared modality [40,41]. We now proved that SHG polarization could provide structural information in proteins. SHG measurements do not require labeling, unlike NMR and FRET, and are therefore applicable to long-term sequential sampling. The present study represents not only an important step toward the creation of a new structural analysis platform, but also an eccentric use of SHG microscopy.

A preliminary version of this work, doi: 10.1101/338137, was deposited in the bioRxiv on June 4, 2018.

Acknowledgement

We are deeply grateful to Kylius Wilkins (RIKEN, BDR) for a critical assessment of this manuscript. We would like to thank Editage (www.editage.com) for English language editing. We also thank Dr. A. Takai and Dr. T. Kambara (RIKEN, BDR), and Dr. H. Inomata (RIKEN, BDR) for the preparation of the *Xenopus* egg extracts and sperm; and S. Xu, J. Asada, and M. Kakiuchi (RIKEN, BDR) for their technical and secretarial assistance. The Kohinoor plasmid was kindly provided by Dr. D. K. Tiwari and Prof. T. Nagai (Osaka University). This work was supported by the Special Postdoctoral Researchers' Program (SPDR) of RIKEN (to J. K. and T. S.); a Grant-in-Aid for JSPS Research Fellows (to J. K.); Grants-in-Aid for Scientific Research (KAKENHI; grant numbers 25871144 to J. K.; 16H05119, 15H01334, 26115721, and 25293046 to Y. O.; and 16H01439 to T. I.) from the Ministry of Education, Culture, Sports, Science, and Technology; the Uehara Memorial Foundation (to Y. O.); the Takeda Science Foundation (to Y. O.); the All RIKEN Research Project on Single Cells (to Y. O. and T. M. W.); and the RIKEN Pioneering Project on Dynamic Structural Biology (to Y. O.).

Conflicts of Interest

The authors declare no competing financial interests.

Author Contributions

T. M. W. and Y. O. conceived the experiments. J. K. built the microscope system and mainly performed the experiments. T. S. and Y. O. designed the microtubule experiments. M. T. and K. I. crystalized the Kohinoor protein. T. I. performed the simulation and supervised the work. T. M. W. designed the project. J. K. and T. M. W. wrote the manuscript with discussion and feedback from all the authors.

References

[1] Binshtein, E. & Ohi, M. D. Cryo-electron microscopy and the amazing race to atomic resolution. *Biochemistry* **54**, 3133–3141 (2015).
[2] Shi, Y. A glimpse of structural biology through X-ray crystallography. *Cell* **159**, 995–1014 (2014).
[3] Callaway, E. The revolution will not be crystallized: a new method sweeps through structural biology. *Nature* **525**, 172–174 (2015).
[4] Levantino, M., Yorke, B. A., Monteiro, D. C., Cammarata, M. & Pearson, A. R. Using synchrotrons and XFELs for time-resolved X-ray crystallography and solution scattering experiments on biomolecules. *Curr. Opin. Struct. Biol.* **35**, 41–48 (2015).
[5] Kovermann, M., Rogne, P. & Wolf-Watz, M. Protein dynamics and function from solution state NMR spectroscopy. *Q. Rev. Biophys.* **49**, e6 (2016).
[6] Schuler, B. & Hofmann, H. Single-molecule spectroscopy of protein folding dynamics—expanding scope and timescales. *Curr. Opin. Struct. Biol.* **23**, 36–47 (2013).
[7] Boyd, R. W. *Nonlinear Optics Third Edition* (Academic Press, Cambridge, 2008).
[8] Pavone, F. S. & Campagnola, P. J. *Second Harmonic Generation Imaging* (CRC Press, Florida, 2013).
[9] Cox, G. Biological applications of second harmonic imaging. *Biophys. Rev.* **3**, 131–141 (2011).
[10] Tiaho, F., Recher, G. & Rouède, D. Estimation of helical angles of myosin and collagen by second harmonic generation imaging microscopy. *Opt. Express* **15**, 12286–12295 (2007).
[11] Rivard, M., Couture, C-A., Miri, A. K., Laliberté, M., Bertrand-Grenier, A., Mongeau, L., *et al.* Imaging the bipolarity of myosin filaments with interferometric second harmonic gen-

eration microscopy. *Biomed. Opt. Express* **4**, 2078–2086 (2013).
[12] Couture, C-A., Bancelin, S., Van der Kolk, J., Popov, K., Rivard, M., Legaré, K., *et al.* The impact of collagen fibril polarity on second harmonic generation microscopy. *Biophys. J.* **109**, 2501–2510 (2015).
[13] Amos, L. A. Microtubule structure and its stabilisation. *Org. Biomol. Chem.* **2**, 2153–2160 (2004).
[14] Moores, C. Studying microtubules by electron microscopy. *Methods Cell Biol.* **88**, 299–317 (2008).
[15] Nogales, E. An electron microscopy journey in the study of microtubule structure and dynamics. *Protein Sci.* **24**, 1912–1919 (2015).
[16] Nogales, E. & Wang, H. W. Structural mechanisms underlying nucleotide-dependent self-assembly of tubulin and its relatives. *Curr. Opin. Struct. Biol.* **16**, 221–229 (2006).
[17] Alushin, G. M., Lander, G. C., Kellogg, E. H., Zhang, R., Baker, D. & Nogales, E. High-resolution microtubule structures reveal the structural transition in αβ-tubulin upon GTP hydrolysis. *Cell* **157**, 1117–1129 (2014).
[18] Yajima, H., Ogura, T., Nitta, R., Okada, Y. Sato, C. & Hirokawa, N. Conformational changes in tubulin in GMPCPP and GDP-taxol microtubules observed by cryoelectron microscopy. *J. Cell Biol.* **198**, 315–322 (2012).
[19] Morikawa, M., Yajima, H., Nitta, R., Inoue, S., Ogura, T., Sato, C., *et al.* X-ray and Cryo-EM structures reveal mutual conformational changes of Kinesin and GTP-state microtubules upon binding. *EMBO J.* **34**, 1270–1286 (2015).
[20] Shima, T., Morikawa, M., Kaneshiro, J., Kambara, T., Kamimura, S., Yagi, T., *et al.* Kinesin-binding-triggered conformation switching of microtubules contributes to polarized transport. *J. Cell Biol.* **217**, 4164–4183 (2018).
[21] Tiwari, D. K., Arai, Y., Yamanaka, M., Matsuda, T., Agetsuma, M., Nakano, M., *et al.* A fast- and positively photoswitchable fluorescent protein for ultralow-laser-power RESOLFT nanoscopy. *Nat. Methods* **12**, 515–518 (2015).
[22] Kaneshiro, J., Watanabe, T. M., Fujita, H. & Ichimura, T. Full control of polarization state with a pair of electro-optic modulators for polarization-resolved optical microscopy. *Appl. Opt.* **55**, 1082–1089 (2016).
[23] Castoldi, M. & Popov, A. V. Purification of brain tubulin through two cycles of polymerization-depolymerization in a high-molarity buffer. *Protein Expr. Purif.* **32**, 83–88 (2003).
[24] Desai, A. & Mitchison, T. J. Preparation and characterization of caged fluorescein tubulin. *Meth. Enzymol.* **298**, 125–132 (1998).
[25] Gard, D. L. & Kirschner, M. W. Microtubule assembly in cytoplasmic extracts of *Xenopus* oocytes and eggs. *J. Cell Biol.* **105**, 2191–2201 (1987).
[26] Psilodimitrakopoulos, S., Petegnief, V., de Vera, N., Hernandez, O., Artigas, D., Planas, A. M., *et al.* Quantitative imaging of microtubule alteration as an early marker of axonal degeneration after ischemia in neurons. *Biophys. J.* **104**, 968–975 (2013).
[27] Nye, J. F. *Physical Properties of Crystals* (OXFORD University Press, Oxford, 1985).
[28] Akhmanova, A. & Steinmetz, M. O. Control of microtubule organization and dynamics: two ends in the limelight. *Nat. Rev. Mol. Cell Biol.* **16**, 711–726 (2015).
[29] Faro, A. R., Carpentier, P., Jonasson, G., Pompidor, G., Arcizet, D., Demachy, I., *et al.* Low-temperature chromophore isomerization reveals the photoswitching mechanism of the fluorescent protein Padron. *J. Am. Chem. Soc.* **133**, 16362–16365 (2011).
[30] Dombeck, D. A., Kasischke, K. A., Vishwasrao, H. D., Ingelsson, M., Hyman, B. T. & Webb, W. W. Uniform polarity microtubule assemblies imaged in native brain tissue by second-harmonic generation microscopy. *Proc. Natl. Acad. Sci. USA* **100**, 7081–7086 (2003).
[31] Kwan, A. C., Dombeck, D. A. & Webb, W. W. Polarized microtubule arrays in apical dendrites and axons. *Proc. Natl. Acad. Sci. USA* **105**, 11370–11375 (2008).
[32] Stoothoff, W. H., Bacskai, B. J. & Hyman, B. T. Monitoring tau-tubulin interactions utilizing second harmonic generation in living neurons. *J. Biomed. Opt.* **13**, 064039 (2008).
[33] Sharoukhov, D. & Lim, H. On probing conformation of microtubules by second-harmonic generation. *J. Mod. Opt.* **63**, 71–75 (2016).
[34] Morita, R. & Yamashita, M. Relationship between second- and third-order nonlinear optical susceptibilities due to electronic polarization. *Jpn. J. Appl. Phys.* **32**, L905–L907 (1993).
[35] Bourgeois, D. & Adam, V. Reversible photoswitching in fluorescent proteins: a mechanistic view. *IUBMB Life* **64**, 482–491 (2012).
[36] Zhou, X. X. & Lin, M. Z. Photoswitchable fluorescent proteins: ten years of colorful chemistry and exciting applications. *Curr. Opin. Chem. Biol.* **17**, 682–690 (2013).
[37] Franken, P. A., Hill, E. A., Peters, C. W. & Weinreich, G. Generation of optical harmonics. *Phys. Rev. Lett.* **7**, 118–119 (1961).
[38] Peleg, G., Lewis, A. Linial, M. & Loew, L. M. Nonlinear optical measurement of membrane potential around single molecules at selected cellular sites. *Proc. Natl. Acad. Sci. USA* **96**, 6700–6704 (1999).
[39] Loew, L. M. & Lewis, A. Second harmonic imaging of membrane potential. *Adv. Exp. Med. Biol.* **859**, 473–492 (2015).
[40] Cohen, B. E. Biological imaging: beyond fluorescence. *Nature* **467**, 407–408 (2010).
[41] Pantazis, P., Maloney, J., Wu, D. & Fraser, S. E. Second harmonic generating (SHG) nanoprobes for in vivo imaging. *Proc. Natl. Acad. Sci. USA* **107**, 14535–14540 (2010).